Combining thermodynamic simulations, element and surface analytics to study U(VI) retention in corroded cement monoliths upon >20 years of leaching

C. Bube, V. Metz *, D. Schild, J. Rothe, K. Dardenne, M. Lagos, M. Plaschke, B. Kienzler

Institute for Nuclear Waste Disposal (KIT-INE), Karlsruhe Institute of Technology, P.O. Box 3640, Karlsruhe 76021, Germany

ARTICLE INFO

Keywords:
Cement corrosion
Uranium(VI) solubility
Thermodynamic simulation
Long-term experiments

ABSTRACT

Retention or release of radionuclides in a deep geological repository for radioactive wastes strongly depends on the geochemical environment and on the interaction with near field components, e.g. waste packages and backfill materials. Deep geological disposal in rock salt is one of the concepts considered for cemented low and intermediate level wastes. Long term experiments were performed to observe the evolution of full scale cemented waste simulates (doped with $(NH_4)_2U_2O_7$) upon reaction with relevant salt brines, e.g. $MgCl_2$ rich and saturated NaCl solutions, and to examine the binding mechanisms of uranium. Throughout the experiments, concentrations of major solution components, uranium and pH values were monitored regularly and compared to thermodynamic equilibrium calculations, which indicate that close to equilibrium conditions have been achieved after 13 14 years duration of the leaching experiments. Two of the full scale cemented waste simulates were recovered from the solutions after 17 18 years and studied by different analytical methods to characterize the solids, especially with respect to uranium incorporation. In drill core fragments of various lateral and horizontal positions of the corroded monoliths, U rich aggregates were detected and analyzed by means of space resolved techniques. Raman, μ XANES and μ XRD analyses of several aggregates demonstrate that they consist of an amorphous diuranate type solid. Within error, calculated U solubilities controlled by Na diuranate ($Na_2U_2O_7{\cdot}H_2O$) are consistent with measured U concentrations in both, the NaCl and the $MgCl_2$ system. Since uranophane occurs also in the corroded monoliths, it is proposed that a transition towards the thermodynamic equilibrium U(VI) phase is kinetically hindered.

1. Introduction

For low and intermediate level radioactive wastes, cementation is commonly used to fix and solidify the heterogeneous waste components. Different concepts exist on an international level for the final disposal of these waste types. In the case of deep geological disposal, one of the issues to be considered within a safety case is the consequence of water contacting the wastes. Low ionic strength ($I < 0.5$ mol (kg H_2O) $^{-1}$) formation waters are found in potential repository sites and underground research laboratories in Korea, Sweden, Switzerland and Finland (crystalline granites/granitoids) as well as in such locations in Belgium, France and Switzerland (argillites), respectively. Numerous studies are concerned with the retention of radionuclides by cementitious materials and their secondary corrosion products upon contact with dilute solutions (Berner, 1992; Ewart et al., 1992; Pointeau et al., 2004; Ritherdon et al., 2003; Wieland et al., 2010). Formation waters, characterized by elevated ionic strength, occur in potential repository sites situated within metamorphic bedrocks in the Canadian Shield and Cretaceous argillites in Northern Germany. In contrast to dilute argillaceous and granitic formation waters, fluid inclusions and brine pockets in rock salt complexes are characterized by high ionic strengths ($I > 5$ mol (kg H_2O) $^{-1}$). In a salt based repository, chloride rich solutions will evolve upon water intrusion and secondary phase precipitates differ from those in dilute systems. There is a strong link between solution composition, the resulting pH values and the solubility limiting solids that are formed.

Thermodynamic calculations are a useful tool for predicting the equilibrium composition of solids and solution under different geochemical conditions. On relatively small time scales, kinetic effects may control the phase composition and hinder a system from reaching its thermodynamic equilibrium. If kinetics are not known, and the experimental data shall be compared to thermodynamic equilibrium calculations, it is therefore essential to conduct the experiments for long enough times to ensure the achievement of an equilibrium state. It is further required to have a reliable

* Corresponding author. Tel.: +49 72160 82 8078; fax: +49 72160 82 4308.
E-mail address: volker.metz@kit.edu (V. Metz).

thermodynamic database including all necessary phases as well as adequate models for the speciation.

Corrosion of cements due to chloride attack has been extensively studied (Arya et al., 1990; Barberon et al., 2005; Loser et al., 2010). Most of the studies were concerned with the mechanical impact of the exposure of cement materials to chloride rich solutions. Since Reardon and co workers studied the cement system under saline conditions and developed a set of Pitzer parameters and solubility constants (Reardon, 1988, 1990, 1992), hardly any other studies were published proposing thermodynamic data for cementitious systems at high ionic strength conditions.

In a previous publication (Bube et al., 2013), long term corrosion of cemented simulated waste products has been described with the focus on describing solution composition and the cementitious solids formed. This work will focus on the retention of U(VI) in these systems in the presence of cement alteration phases after long term leaching in chloride rich solutions. The considered data is from long term corrosion experiments that were conducted in a former rock salt mine. Full scale experiments using cemented waste simulates (200 L sized monoliths) were doped with ^{238}U and exposed to $MgCl_2$ and NaCl rich brines. As described in Bube et al. (2013) and Kienzler et al. (2010), solution composition and pH were measured regularly for up to 22 years and some of the experiments were stopped for solid phase analyses. Results of bulk solid phase analysis of powdered samples with TRLFS, XANES and XRD were presented earlier (Kienzler et al., 2010). In this work, Raman microspectroscopy, μ XAFS and μ XRD are applied to U rich aggregates that were identified on the core samples by SEM backscattering, SEM EDX and visual analyses. In two recent conference proceedings we reported preliminary results of our studies on the U(VI) retention in the corroded monoliths (Bube et al., 2011; Rothe et al., 2013). The present study is an extension of these studies, dealing with additional experimental systems and refined analytical and theoretical approaches, respectively. The experimental results on solution compositions and solid U(VI) phases are compared to thermodynamic equilibrium calculations.

2. Materials and methods

2.1. Full scale experiments

The cemented waste product simulates were produced in the 1980s by the former Institut für Tieflagerung, Braunschweig (Germany). The waste concentrates were composed corresponding to the composition of chemical residues from reprocessing of spent nuclear fuel with the PUREX process (Vejmelka et al., 1990). The cement monoliths #31, #32, #33 and #34 considered in this study were prepared from Ordinary Portland Cement (OPC, CEM I 42,5 R) with a load of 11 wt.% process chemicals in 200 L steel drums at a water cement ratio of $W/C = 0.5$. The major component of the waste simulate was $NaNO_3$ (9 wt.%), while minor constituents included $Na_2HPO_4\ 12H_2O$, Na citrate, Na tartrate and Na oxalate (for details on the composition of the simulates see Bube et al. (2013)). Each of the four monoliths had a mass of 336 kg and were doped with 1.017 kg $(NH_4)_2U_2O_7$. After their complete hydration the monoliths were transferred into 400 L steel drums filled with either NaCl rich brine (#31 and #32) or $MgCl_2$ rich brine (#33 and #34). The two experiments in NaCl rich brine were started in November 1988, the ones in $MgCl_2$ rich brine were started in September 1989. Initial composition of the leachants is shown in Table 1. After 18 and 17 years, monolith #31 and #33 were recovered from the solutions and core samples were retrieved by vertical drilling.

2.2. Analytical methods

Optical emission spectrometry with a Perkin Elmer ICP OES Optima 4300 DV was used to measure Ca, Mg, Na, and K concentrations in solution. Aliquots were diluted 1:20,000 before Ca measurements, 1:1000 before Na measurements and 1:1000 before Mg and K measurements. Detection limits of the Ca, Mg, Na and K analysis were 0.5, 0.8, 8.7 and 5.1 mmol L^{-1}, respectively. Precision of the analyses were in the range of ±4% for Mg and ±12% for Na and K (determined from relative standard deviation, RSD). Dissolved Si, Al, Fe and U were analyzed by mass spectrometry using an ICP MS Perkin Elmer ELAN 6100. Measured Si, Al and Fe concentrations were below the detection limits of 1.0, 3.7 and 0.3 mmol L^{-1}, respectively. The detection limit of ^{238}U was 1×10^{-10} mol L^{-1}. The precision of U concentrations measured in the full scale experiment was less than 4% (RSD). Chloride, nitrate and sulfate were measured by ion chromatography using a DX300 Dionex. For a dilution factor of 1000, detection limits of the chloride, nitrate and sulfate analyses were at 2.8, 1.6 and 1.0 mmol L^{-1}, respectively. The precision of chloride (dilution factor 10), nitrate (dilution factor 5000) and sulfate (dilution factor 20,000) measurements was in the range of ±5% for chloride and ±30% for sulfate.

The pH of the solutions was measured with a ROSS semi micro combination electrode and ORION pH meter 720 A having an estimated accuracy of ±0.1 pH units. In high ionic strength solutions ($I > 0.1$ m), measured pH values, pH_{exp}, are not defined anymore and were therefore converted into H^+ concentrations ($-\log m(H^+) = pH_m$) as described in Altmaier et al. (2003, 2008). Pure and mixed $MgCl_2$, $CaCl_2$ and NaCl solutions with known H^+ concentrations were used to derive the conversion parameters ($A = pH_m - pH_{exp}$). The resulting A values were related to the solution composition by polynomial fitting so that the A value could be calculated for given $MgCl_2$, $CaCl_2$, and NaCl concentrations measured in the long term experiments (as an approximation, the KCl concentration was added to the NaCl concentration). Accuracy for this pH_m determination is estimated as ±0.25 units resulting from uncertainties in measured Mg, Ca, Na and Cl, in addition to unaccounted effects of minor solutes on the value of A.

Drill dust and core fragments sampled from the corroded monoliths #31 and #33 were analyzed using Raman microspectroscopy, scanning electron microscope energy dispersive spectrometry (SEM EDX) and X ray diffraction (XRD). Raman spectra were measured with a BRUKER Senterra Raman microscope operated with depolarized 5 and 25 mW laser beams at 532 nm and 785 nm excitation wavelengths, respectively. SEM EDX analyses were carried out with a CamScan FE44 instrument. XRD measurements were performed using a Bruker D8 variance diffractometer equipped with a Cu radiation tube, Ni filters and a Sol X detector. Drill dust samples, approximately 100 mg per aliquot, were digested in a crucible with a hot HCl HF acid mixture, fumed and afterwards redigested in HNO_3. The acidic solutions were analyzed with a Thermo Scientific Element XR Sector Field ICP MS. Commercially available cement reference material (SX 02 02 containing 6.2 ± 0.2 ppm U; prepared by Dillinger Hütte) was used to evaluate the accuracy of U measurements. The concentration was determined with an analytical uncertainty in the range of 0.6 6.4% (RSD).

Synchrotron radiation based methods were used to advance the studies that had been performed previously with bulk powder samples (Kienzler et al., 2010). In drill core thin sections, regions of interest were preselected using SEM backscattering images and visible light microscopy images. The ANKA INE Beamline was used for spatially resolved μ XRD and μ XANES measurements (Rothe et al., 2012). Diffraction patterns were recorded on erasable X ray sensitive films (Perkin Elmer). A polycapillary optic was selected for recording μ XAFS spectra at the U L3 edge. This

Table 1
Initial composition of the NaCl-rich and $MgCl_2$-rich leachants and final solution compositions of experiments with monoliths #31, #32 (starting with NaCl brine) and #33, #34 (starting with $MgCl_2$-rich brine).

Solute mol (kg H_2O) [1]	NaCl-brine Initial	#31 (Average) 17.5 years	#32 (Average) 22.2 years	$MgCl_2$-brine Initial	#33 (Average) 16.6 years	#34 (Average) 21.4 years
Mg^{2+}	4×10^{2}	b.d.l.	b.d.l.	4.1	1×10^{2}	$<1 \times 10^{3}$
Ca^{2+}	3×10^{2}	1×10^{2}	1×10^{2}	1×10^{4}	<3.8	2.2
Na^{+}	6.1	6.2	>5.6	4×10^{1}	3.3	3.2
K^{+}	4×10^{2}	0.7	3×10^{1}	7×10^{1}	n.d.	7×10^{1}
U (total)	n.d.	2×10^{7}	1×10^{7}	n.d.	7×10^{7}	4×10^{7}
Si (total)	n.d.	b.d.l.	b.d.l.	n.d.	b.d.l.	b.d.l.
Cl	6.2	5.7	5.8	8.7	7	5.5
SO_4^{2}	5×10^{3}	6×10^{2}	6×10^{2}	3×10^{1}	3×10^{3}	3×10^{3}
NO_3	n.d.	1.4	1.3	n.d.	<2.5	1.9
pH_m	~7	13.1	12.9	n.d.	12.2	11.7

n.d. – Not determined; b.d.l. – below detection limit.

Table 2
Solubility and complex stability constants of relevant U(VI) solids and aqueous species.

	$\log \beta^{\circ}$	Source
Aqueous U(VI) species		
$UO_2^{2+} + H_2O \rightleftharpoons UO_2(OH)^{+} + H^{+}$	−5.25	Guillaumont et al. (2003)
$UO_2^{2+} + 2H_2O \rightleftharpoons UO_2(OH)_2(aq) + 2H^{+}$	−12.15	Guillaumont et al. (2003)
$UO_2^{2+} + 3H_2O \rightleftharpoons UO_2(OH)_3^{-} + 3H^{+}$	−20.25	Guillaumont et al. (2003)
$UO_2^{2+} + 4H_2O \rightleftharpoons UO_2(OH)_4^{2-} + 4H^{+}$	−31.92	Neck et al. (2003)
$2\ UO_2^{2+} + 2\ H_2O \rightleftharpoons (UO_2)_2(OH)_2^{2+} + 2\ H^{+}$	−5.62	Guillaumont et al. (2003)
$3UO_2^{2+} + 2H_2O \rightleftharpoons (UO_2)_3(OH)_4^{2+} + 4H^{+}$	−11.9	Guillaumont et al. (2003)
$3UO_2^{2+} + 5H_2O \rightleftharpoons (UO_2)_3(OH)_5^{+} + 5H^{+}$	−15.55	Guillaumont et al. (2003)
$3UO_2^{2+} + 7H_2O \rightleftharpoons (UO_2)_3(OH)_7^{-} + 7H^{+}$	−32.2	Guillaumont et al. (2003)
$4UO_2^{2+} + 7H_2O \rightleftharpoons (UO_2)_4(OH)_7^{+} + 7H^{+}$	−21.9	Guillaumont et al. (2003)
	$\log K^{\circ}$	
U(VI) solids		
$UO_2^{2+} + 3H_2O \rightleftharpoons UO_3:\ 2H_2O + 2H^{+}$	−5.34	Neck et al. (2003)
$UO_2^{2+} + 2H_2O \rightleftharpoons \beta\text{-}UO_2(OH)_2 + 2H^{+}$	−4.93	Guillaumont et al. (2003)
$2UO_2^{2+} + 2Na^{+} + 4H_2O \rightleftharpoons Na_2U_2O_7 \cdot H_2O + 6H^{+}$	−24.38	Neck et al. (2003)
$2UO_2^{2+} + Ca^{2+} + 6H_2O \rightleftharpoons CaU_2O_7 \cdot 3H_2O + 6H^{+}$	−23.4[a]	Altmaier et al. (2005)
$2UO_2^{2+} + Ca^{2+} + 5H_2O + 2H_4SiO_4 \rightleftharpoons Ca(UO_2)_2(SiO_3OH)_2 \cdot 5H_2O + 6H^{+}$	−9.42	Guillaumont et al. (2003)

[a] Note that data was evaluated with the SIT equation; Pitzer parameters unknown.

optic refocussed monochromatic radiation delivered by a double crystal monochromator (DCM) equipped with a pair of Ge < 422 > crystals and the toroidal second beamline mirror into a spot size of 25 to 30 μm at the sample surface. U L3 μ XAFS spec tra, recorded in fluorescence yield detection mode, were normal ized to the total flux impinging on the sample measured by a pin diode mounted behind the polycapillary. The DCM energy was calibrated relative to the first inflection point in the K XANES of a Y foil defined as 17.038 keV. Details are given in (Rothe et al., 2013).

2.3. Thermodynamic database and simulations

Thermodynamic equilibrium calculations were done with "The Geochemist's Workbench" (GWB) software package (Bethke and Yeakel, 2009) using the Pitzer approach (Pitzer, 1973) for activity calculations to account for the high ionic strength of the systems. Solubility limited U(VI) concentrations were calculated from the measured elemental composition of the solutions at different times. U(VI) concentrations were calculated for different U(VI) sol ids that may be present. The thermodynamic data is based on the data evaluation of Harvie et al. (1984), which is extended for Si (Reardon, 1992) and Al aqueous species (Hummel et al., 2002) and Pitzer parameters reported in Reardon (1988, 1990). Data for the relevant solid phases of the cement system is taken from var ious sources (Lothenbach and Winnefeld, 2006; Matschei et al., 2007; Reardon, 1992; Robie and Hemingway, 1995; Stronach and Glasser, 1997; Wolery, 1992). For details on the thermodynamic database the reader is referred to Bube et al. (2013). Solubility and complex stability constants of relevant U(VI) solids and aque ous species (given in Table 2) were taken from Guillaumont et al. (2003) and from Altmaier and Neck (Altmaier et al., 2005; Neck et al., 2003). Pitzer parameters of U(VI) species originate from Pit zer (1991) and Plyasunov et al. (1998) as well as from Neck et al. (2003) who derived a parameter set from a correlation of SIT and Pitzer parameters following an approach of Grenthe and Plyasuno va (1997) and Plyasunov et al. (1998). Pitzer parameters for inter actions of Ca^{2+} with U(VI) aqueous species are not available.

3. Results

3.1. Solution composition

In the $MgCl_2$ systems (experiments #33 and #34) the brine composition continuously changed within the first 11.6 years from concentrated $MgCl_2$ solution with initial near neutral pH to a $CaCl_2$ NaCl rich solution with pH_m values around 12. Approxi mately half of the $NaNO_3$ inventory was leached from the

cemented waste simulates within this period. Measured U concentrations were around 10^{-7} mol (kg H_2O)$^{-1}$ (molal, *m*) after 4–5 years, while after 8 years, lower U concentrations of 3×10^{-9} to 4×10^{-8} *m* were detected. Following this, concentrations increased again until, after 13.6 years, they reached concentrations between 10^{-6} and 10^{-7} m. The temporal evolution of the major dissolved species, U and the pH_m is shown in Bube et al. (2013); averaged concentrations of the last samplings are given in Table 1. The observed increase in U concentrations between 8 and 13.6 years after the start of the experiments developed in parallel to the increase of pH values. Between 13.6 and 21.4 years, the concentrations of the major solution components and the pH_m remained at a constant level. Uranium concentrations seem to be closely coupled to the evolution of the solution composition, in particular to the pH_m values. Fig. 1 displays concentrations of dissolved uranium as function of pH_m values measured in experiments with initial NaCl rich solution (#31 and #32) and in those with initial $MgCl_2$ rich solution (#33 and #34) (data of (Kienzler et al., 2010)). In the NaCl systems (experiments #31 and #32), changes in the solution composition were less pronounced than in the $MgCl_2$ system, even if pH_m increased from an initial value of 8 to values around 13. After an initial increase in NaCl concentration from 6 *m* to 7–8 *m* after 12.5 years, concentrations decreased again to values around the initial concentrations. Mg and Ca concentrations remained low at all times, while nitrate and K concentrations increased to values around 1.0–2.0 *m* and ~0.7 *m* after 18 years. Nitrate concentrations after 22.2 years were thus slightly lower than those measured in the $MgCl_2$ system (~2 *m* after 21.4 years). Measured U concentrations were around 10^{-8} *m* after 4 to 5 years, one logarithmic unit lower than in the $MgCl_2$ systems. After that, U concentrations increased up to 5×10^{-7} *m* after 17.5 years. In experiment #32, which was performed up to 22.2 years, this was followed by a decrease to values between 10^{-8} and 10^{-7} m. In the case of NaCl rich leaching solution, major dissolved aqueous species and pH_m values were virtually constant after 14.5 to 22.2 years. Averaged concentrations of the last samplings of experiments #31 and #32 are given in Table 1, and the temporal evolution of the solution composition is shown in Bube et al. (2013). A similar correlation between pH_m and U(VI) concentrations is observed as in the case of $MgCl_2$ rich solution (Fig. 1)

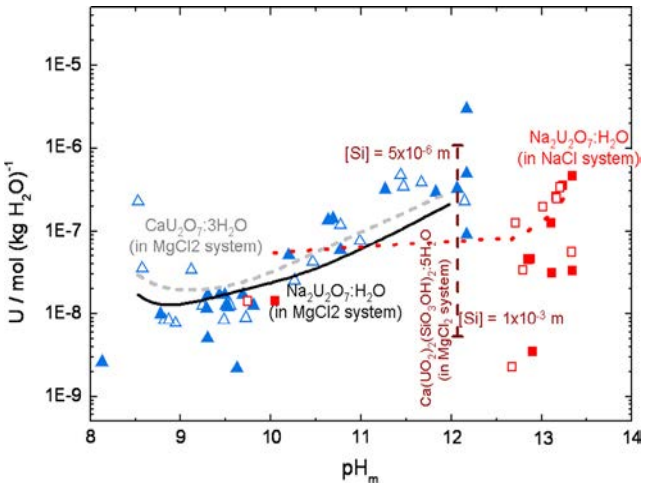

Fig. 1. Concentrations of dissolved uranium as function of pH_m values measured in experiments with initial NaCl rich solution (#31 and #32) and in experiments with initial $MgCl_2$ rich solution (#33 and #34) compared to calculated solubilities of uranophane, Ca- and Na-diuranate. Open and closed squares denote measurements in #31 and #32, respectively; open and closed triangles denote measurements in #33 and #34, respectively (data of Kienzler et al., 2010). Lines depict thermodynamic solubility calculations for equilibrium with Ca-diuranate ($CaU_2O_7 \cdot 3H_2O$; grey dashed line), Na-diurante ($Na_2U_2O_7 \cdot H_2O$; black solid line) and uranophane ($Ca(UO_2)_2(SiO_3OH)_2 \cdot 5H_2O$); vertical dashed line) in the $MgCl_2$ system as well as Na-diurante ($Na_2U_2O_7 \cdot H_2O$; dotted line) in the NaCl system.

3.2. Composition of the solid phase

As it is explained in detail in Bube et al. (2013), solids sampled from corroded monolith #33 ($MgCl_2$ system) contain brucite, gypsum, calcite, halite, hydrotalcite and/or Friedel's salt and traces of ettringite. Samples from monolith #31 (recovered from the NaCl system) contain mainly calcite, portlandite and halite. In both systems, these solid phases are found homogeneously distributed within the top 50 cm.

Uranium concentrations were measured in drill dust specimens of 100 mg sampled in various lateral and vertical positions of the monoliths. The drill dust samples were digested and analyzed by means of ICP MS. The average U concentration of 2860 ± 325 ppm measured in 22 samples of the corroded monolith #31 is within error equal to the initial U doping of the cemented waste simulate (i.e. 3030 ppm). The average U concentration measured in 15 samples of the corroded monolith #33 is in the same range (3170 ppm), however the large standard deviation of ±1460 ppm reflects a considerable scatter in the U distribution in the monolith. A profile of the U concentrations measured in samples from different depths within monolith #33 (0–10 cm up to 40–50 cm depth) reveals a heterogeneous distribution of the uranium in the $MgCl_2$ system (Fig. 2), which is attributed to insufficient mixing during the preparation of the cement paste and addition of the ammonium diuranate (Kienzler et al., 2010).

In drill core fragments from the top 50 cm of monoliths #33 and #31, U rich aggregates were detected by SEM–EDX. In the uppermost sample (0–10 cm depth), these aggregates contain up to 10 atom% uranium and are sized between 5 and 100 µm. The sizes of U rich aggregates are between 1 and 20 µm in drill core fragments of lower positions. Several of the U rich aggregates were studied by Raman microspectroscopy. Spectra of the aggregates (see Fig. 3) display considerable similarities even if from different lateral and vertical positions. These Raman spectra were then compared to reference spectra of different U(VI) minerals from the RRUFF database (RRUFF, 2013). Best agreement is found with the reference spectra of diuranates, $CaU_2O_7 \cdot 3H_2O$(cr) and $Na_2U_2O_7 \cdot H_2O$, whereas spectra of uranophane (Fig. 3), coffinite (RRUFF #070402), blatonite (RRUFF #060594), rutherfordine (RRUFF #090018), schoepite (RRUFF #080082) and soddyite (RRUFF #060361) show significantly different signals. Signals at wavenumbers between 1020 and 1090 cm^{-1} that are observed in all spectra are interpreted as interferences with

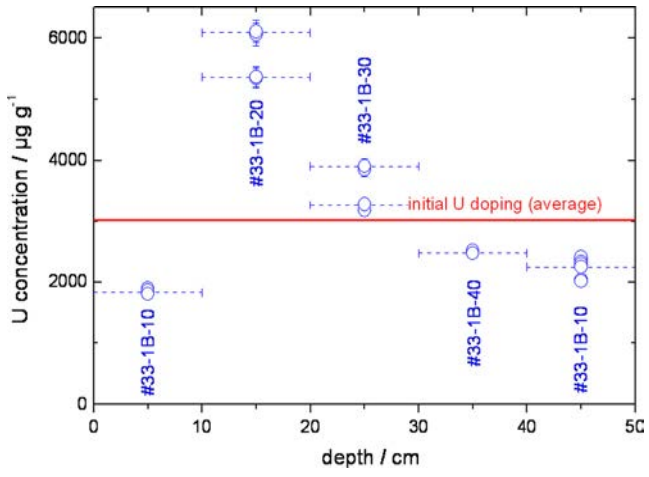

Fig. 2. U concentrations in drill dust aliquots of monolith #33 as function of the sampling depth. For comparison, initial U doping of monolith #33 is indicated by a line.

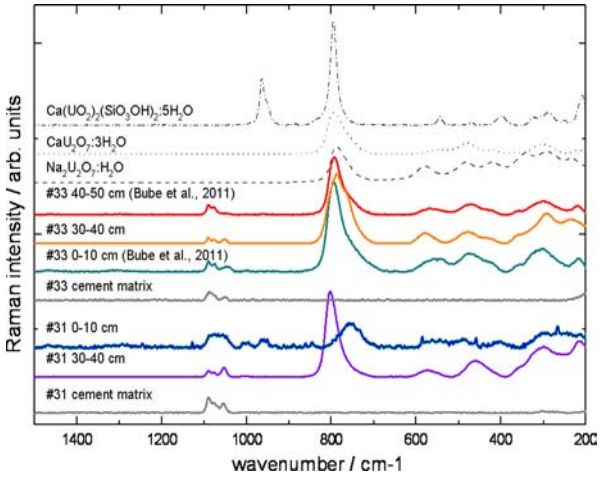

Fig. 3. Exemplary Raman spectra of U-rich aggregates sampled from various positions in the corroded monoliths #31 and #33. Data of U-rich aggregates sampled in monolith #33 at a depth of 0–10 cm and 40–50 cm are taken from Bube et al. (2011). For comparison spectra of the cement matrix next to the U-rich aggregate of monoliths #31 and #33 (sampled in a depth of 30–40 cm and 40–50 cm, resp.) as well as reference spectra of uranophane/$Ca(UO_2)_2(SiO_3OH)_2{\cdot}5H_2O$ (sample provided by N. Macé), Ca-diuranate/$CaU_2O_7{\cdot}3H_2O$ and Na-diuranate/$Na_2U_2O_7{\cdot}H_2O$ are shown. Raman spectra (vertically shifted for clarity) were recorded at an excitation wavelength of 785 nm.

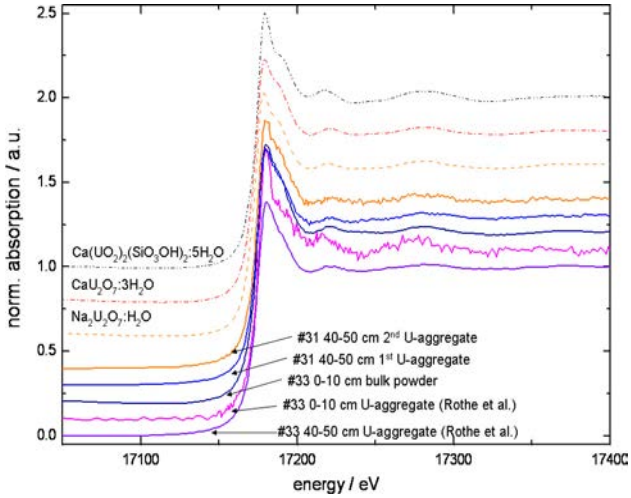

Fig. 4. U L3 XANES spectrum of bulk powder (sampled of monolith #33 at a depth of 0–10 cm) compared to respective μ-XANES spectra of U-rich aggregates of monolith #31 (sampled at a depth of 40–50 cm) and of mononolith #33 (sampled at a depth of 0–10 cm and 40–50 cm; data of Rothe et al. (2013)). For comparison reference spectra of uranophane/$Ca(UO_2)_2(SiO_3OH)_2{\cdot}5H_2O$ (sample provided by N. Macé), Ca-diuranate/$CaU_2O_7{\cdot}3H_2O$ and Na-diuranate/$Na_2U_2O_7{\cdot}H_2O$ are shown. Spectra are vertically shifted for clarity.

carbonate rich cement alteration phases. Fig. 3 shows two exem plary spectra of the U free cement matrix next to U rich aggregates of monoliths #31 and #32. The spectra of the cement matrix display the signals in the range of 1020 and 1090 cm ^{1}, too. Though, signals at these wavenumbers are also observed in reference spectra of uranium carbonate minerals, e.g. andersonite ($Na_2Ca(UO_2)(CO_3)_3$ $6H_2O$), liebigite ($Ca_2(UO_2)(CO_3)_3$ $11H_2O$) (RRUFF #050662.2) or zellerite ($Ca(UO_2)(CO_3)_2$ $5H_2O$), the main lines of these minerals at wavenumbers higher than 820 cm ^{1} are not found in the spectra of the studied drill core fragments.

In their earlier work, Kienzler et al. (2010) applied laser spec troscopy and U L3 XANES to identify the U solid in bulk powder samples. Hints were found for the presence of a crystalline urano phane like phase. Synchrotron radiation based techniques were combined in the present study to analyze the U rich aggregates that were identified by means of Raman microspectroscopy and SEM EDX. Different samples from both monoliths (#31 and #33) collected at 0 10 cm depth and 40 50 cm depth were analyzed by μ XAFS and μ XRD methods. Surprisingly, μ XRD measure ments of the U rich aggregates exhibit no clear evidence for the presence of a crystalline uranium phase. It is emphasized that the U(VI) phase detected in the aggregates is amorphous. All U rich aggregates generally exhibit U L3 XANES energy positions that are characteristic for U(VI). Features in μ XANES spectra obtained for most of the U rich aggregates are nearly indistinguishable from each other and from previously recorded spectra of bulk samples (Fig. 4). According to Rothe et al. (2013), some of the features exhibited in the μ XANES spectra deviate from those of typical U(VI) dioxo moieties (e.g. metaschoepite $(UO_2)_8O(OH)_{12}$ $12H_2O$, uranophane $Ca(UO_2)_2(SiO_3OH)_2$ $5H_2O$) and are more in accordance with the assumption of a diuranate type solid (e.g. $Ca_2U_2O_7$ $3H_2O$/ $Na_2U_2O_7$ H_2O). Generally, U L3 μ XANES spectra obtained for U aggregates in monoliths #31 and #33 resemble those of diuranate reference samples. Yet, at least one aggregate found in a sample obtained from #33 at 0 10 cm depth exhibits features that are characteristic for a uranophane like U(VI) phase (Fig. 4).

3.3. Thermodynamic simulations

The decrease of Mg^{2+} concentrations and increase of Ca^{2+} con centrations with increased reaction of cement observed in the experiments with $MgCl_2$ rich leaching solutions is also obtained in the thermodynamic calculations (Bube et al., 2013). The concen trations of the major solutes (that were calculated for the respec tive cement mass to brine volume, m/V, ratios) are close to the experimental values at steady state after 13 to 21.4 years. Since U rich aggregates are present at different lateral and vertical posi tions of monoliths #31 and #33, U concentrations are considered to be controlled by solubility phenomena. Solubilities of different U(VI) minerals that were previously reported to occur in cementi tious systems (Moroni and Glasser, 1995; Ritherdon et al., 2003) were calculated for model solutions composed similar to the experimental solutions at different times during the leaching experiments. For both systems, solubilities of becquerelite (CaU_6 O_{19} $11H_2O$), metaschoepite (UO_3 $2H_2O$) and soddyite ($(UO_2)_2SiO_4$ $2H_2O$) are more than one order of magnitude higher than mea sured U concentrations. Considering the solubility constant of clarkeite ($Na(UO_2)O(OH)$, i.e. $Na_2U_2O_7$ H_2O) determined by Gor man Lewis et al. (2008), relatively low U concentrations around 1×10^{11} m were calculated. Due to the fact that experimental Si concentrations are below the detection limit of 1×10^{3} m it is not possible to calculate solubilities in equilibrium with urano phane ($Ca(UO_2)_2(SiO_3OH)_2$ $5H_2O$)) for the analytically determined solution compositions. According to the thermodynamic simula tion of the cement alteration in the brine, Si concentrations are in the range of 5×10^{6} and $\sim 10^{-4}$ m (Bube et al., 2013). Consider ing these Si concentrations, measured U concentrations in the $MgCl_2$ system are in agreement with those predicted at equilib rium with uranophane as solubility controlling U(VI) phase (Fig. 1). In the NaCl system, measured Ca concentrations are much lower than in the $MgCl_2$ system so that U concentrations, consid ered to be controlled by uranophane, would be at least one order of magnitude higher than the experimental values. For Ca diura nate ($Ca_2U_2O_7$ $3H_2O$), the case is similar. In the $MgCl_2$ systems measured and calculated U concentrations are in agreement within error, but in the NaCl system U concentrations predicted for equi librium with Ca diuranate are around one order of magnitude higher than the experimental values (Fig. 1). However, the calcu lated Ca diuranate and uranophane solubilities are only tentative approximations because presently no Pitzer parameters are avail able for interactions of aqueous U(VI) species with Ca^{2+}. Within error, calculated U solubilities controlled by Na diuranate

($Na_2U_2O_7\ H_2O$) are consistent with measured U concentrations in both, the NaCl and the $MgCl_2$ system (Fig. 1).

4. Discussion

In their work, Kienzler et al. (2010) studied drill dust samples of monoliths #31 (corroded in NaCl rich brine) and #33 (corroded in $MgCl_2$ rich brine) using XANES, TRLFS and XRD. All three methods concordantly give hints on the presence of a crystalline urano phane like U(VI) phase. In this work, relatively large U rich aggre gates with a size of 1 and 100 μm are studied, which were taken from various lateral and vertical positions of the corroded mono liths #31 and #33. Raman μ spectroscopy, SEM EDX, μ XRD and μ XAFS measurements are used to get information on the solid U(VI) phase these aggregates are composed of. According to μ XRD, these U rich aggregates are amorphous. Raman spectra of these aggregates closely match to Ca and Na diuranate reference spectra. μ XAFS measurements of various U rich aggregates, sam pled from various positions of monoliths #31 and #33, are indistin guishable, which leads to the hypothesis that a singular U(VI) phase is present in the U rich aggregates. In accordance with the results of Raman μ spectroscopy, U L3 XANES patterns of the aggregates resemble to respective spectra of diuranate type phases. However, at least one of the spectra obtained from an aggregate sampled from monolith #33 shows different characteris tics that are more typical for a uranophane like U(VI) phase. This indicates that there may be more than one U(VI) mineral present in the solid.

Based on the results of bulk powder analyses of Kienzler et al. (2010) and the μ spectroscopic analyses of the relatively large U rich aggregates, it is concluded that crystalline uranophane occurs together with an amorphous diuranate type solid, the latter one dominates the relatively large aggregates. Since the diuranate is not crystalline, it is not observed in the XRD analyses of Kienzler et al. (2010). In contrast to the monolith corroded in NaCl brine, uranium is not homogeneously distributed within monolith #33 ($MgCl_2$ system), which is attributed to incomplete mixing during the monolith fabrication. These observations lead to the conclusion that for the trace component uranium, local and partial equilibria have been achieved rather than a complete equilibrium in the full scale experiments even after two decades. The close to equi librium conditions are simulated by means of thermodynamic equilibrium calculations considering an equilibrium between a pure U(VI) solid phase and the U(VI) in the aqueous phase. Alterna tively, one may consider the formation of solid solutions of U(VI) and a hosting mineral of the corroded cement matrix. Gaona et al. (2012) developed a model for an aqueous solid solution equilibrium controlling the uptake of U(VI) in C S H phases under low ionic strength conditions. They compared experimentally determined R_d values of U(VI) in C S H phases, various OPC types, OPC/PFA mixtures and "cement zone" material of the Maqarin nat ural analogue site to R_d simulations of the aqueous solid solution model. The aqueous U concentrations measured in the present study correspond to R_d values of 10^6 L kg $^{-1}$ at $pH_m \sim 10$ and 10^4 to 10^5 L kg $^{-1}$ at $pH_m \sim 12$ in the $MgCl_2$ system, and 10^4 to 10^6 L kg $^{-1}$ at $pH_m \sim 13$ in the NaCl system, respectively. These R_d val ues are close to or within the range of R_d values predicted by Gaona et al. (2012). Since the model of Gaona et al. (2012) is developed for low ionic strength systems and does not include ion interaction parameters for the highly concentrated solutions of the present study, an application of the model is not feasible. A retention of U(VI) in C S H phases is not considered for the monoliths after the long time exposure to $MgCl_2$ rich brine and NaCl brine, because the C S H phases of the monoliths transferred into alteration phases. Therefore it is concluded, that the aqueous U concentration is controlled by the solubility of U(VI) phases rather than by solid solution/sorption phenomena.

Simulations performed for U(VI) solubility equilibria with Na diuranate result at uranium concentrations in the range of the measured ones. However, the U solubility in equilibrium with uranophane cannot be uniquely calculated due to the uncertain Si concentration which results from the high Si detection limit in the brines. In the $MgCl_2$ system, the presence of an uranophane type solid might also lead to U concentrations in the range of the measured concentrations. However, Pitzer parameters for U inter actions with Si and Ca are not available so that the results for ther modynamic solubilities of uranophane and Ca diuranate can only be regarded as an approximation.

5. Conclusions

As described in detail in Bube et al. (2013), the observed evolution of the solution composition with time and the concor dance of measured steady state solution compositions with thermodynamic equilibrium calculations indicate that close to equilibrium conditions are achieved within 13 14 years both in the cemented waste simulates corroded in $MgCl_2$ rich brine and those corroded in NaCl rich brine. U concentrations measured after 13 to 21.5 years are virtually constant with time. This allows to assume that a metastable equilibrium between the bulk solution and a dominating U(VI) solid phase is achieved. Thermodynamic simulations of the solubilities of different U(VI) phases show that in equilibrium with Na diuranate/$Na_2U_2O_7\ H_2O$, U concentrations would be in the range of the measured ones in both $MgCl_2$ and NaCl system. Presence of uranophane in the $MgCl_2$ system would also result in U concentrations close to the measured ones but clearly higher than the measured ones in the case of the NaCl system. Raman and μ XANES spectra of several amorphous U rich aggregates from monoliths #31 and #33 closely resemble those of Na and Ca diuranate reference spectra. The detection of urano phane in bulk powder samples (Kienzler et al., 2010) and in a single U rich aggregate indicates that a transition towards the thermody namic equilibrium phase is kinetically hindered. This hypothesis implies that one of the potentially two U(VI) solids still undergoes slow conversion towards the thermodynamically stable phase while the overall system approached close to equilibrium condi tions. Since the concentrations of U measured in solution are close to solubilities of $Na_2U_2O_7\ H_2O$ (both in the $MgCl_2$ and in the NaCl system) and below solubilities of uranophane and $CaU_2O_7\ 3H_2O$, it is concluded that the effect of the major component $NaNO_3$ (9 wt.%) and those of potentially complexing constituents, such as Na citrate, Na tartrate and Na oxalate, are negligible under the studied conditions.

Acknowledgments

The authors would like to thank our colleagues at KIT INE, in particular E. Bohnert, M. Böttle, F. Geyer, M. Schlieker, E. Soballa and C. Walschburger for performing the (radio)chemical analyses and technical assistance during SEM EDX analyses; M. Altmaier, M. Denecke and T. Vitova are ackowledged for fruitful discussions regarding thermodynamics of the U(VI) solubility phases and inter pretation of the synchrotron based studies, respectively. The valu able comments of X. Gaona as well as thorough reviews by E. Wieland (PSI) and two anonymous reviewers are gratefully acknowledged. We thank N. Macé (formerly at PSI) for providing an uranophane reference sample. The research leading to these re sults has been financially supported in part from the German Fed eral Office for Radiation Protection (BfS) within the projects "Analyse der Eigenschaften von simulierten, zementierten 1:1

Gebinden und ihres Phasenbestandes nach 20 Jahren Auslaugung in Salzlösungen".

References

Altmaier, M., Metz, V., Neck, V., Müller, R., Fanghänel, T., 2003. Solid-liquid equilibria of $Mg(OH)_2$(cr) and $Mg_2(OH)_3Cl{\cdot}4H_2O$(cr) in the system Mg-Na-H-OH-O-Cl-H_2O at 25 °C. Geochim. Cosmochim. Acta 67, 3595–3601.

Altmaier, M., Neck, V., Müller, R., Fanghänel, T., 2005. Solubility of U(VI) and formation of Ca2U2O7:3H2O(cr) in alkaline CaCl2 solutions, International Conference on Chemistry and Migration Behaviour of Actinides and Fission Products in the Geosphere, Migration '05, Avignon, France.

Altmaier, M., Neck, V., Fanghänel, T., 2008. Solubility of Zr(IV), Th(IV) and Pu(IV) hydrous oxides in $CaCl_2$ solutions and the formation of ternary Ca-M(IV)-OH complexes. Radiochim. Acta 96, 541–550.

Arya, C., Buenfeld, N.R., Newman, J.B., 1990. Factors influencing chloride-binding in concrete. Cem. Concr. Res. 20, 291–300.

Barberon, F., Baroghel-Bouny, V., Zanni, H., Bresson, B., de la Caillerie, J.-B., Malosse, L., Gan, Z., 2005. Interactions between chloride and cement-paste materials. Magn. Reson. Imag. 23, 267–272.

Berner, U.R., 1992. Evolution of pore water chemistry during degradation of cement in a radioactive waste repository environment. Waste Manage. 12, 201–219.

Bethke, C.M., Yeakel, S., 2009. The Geochemist' s Workbench. University of Illinois, Urbana, USA.

Bube, C., Metz, V., Schild, D., Lagos, M., Bohnert, E., Garbev, K., Altmaier, M., Kienzler, B., 2011. Interactions of U(VI) with cement alteration products in highly saline solutions. In: Société Francaise d'Energie Nucléaire (SFEN) (Ed.), NUWCEM 2011, 1st International Symposium on Cement-based Materials for Nuclear Wastes, Avignon (France).

Bube, C., Metz, V., Bohnert, E., Garbev, K., Schild, D., Kienzler, B., 2013. Long-term cement corrosion in chloride-rich solutions relevant to radioactive waste disposal in rock salt – leaching experiments and thermodynamic simulations. Phys. Chem. Earth 64, 87–94.

Ewart, F.T., Smith-Briggs, J.L., Thomason, H.P., Williams, S.J., 1992. The solubility of actinides in a cementitious near-field environment. Waste Manage. 12, 241–252.

Gaona, X., Kulik, D.A., Macé, N., Wieland, E., 2012. Aqueous-solid solution thermodynamic model of U(VI) uptake in C-S-H phases. Appl. Geochem. 27, 81–95.

Gorman-Lewis, D., Fein, J.B., Burns, P.C., Szymanowski, J.E.S., Converse, J., 2008. Solubility measurements of the uranyl oxide hydrate phases metaschoepite, compreignacite, Na-compreignacite, becquerelite, and clarkeite. J. Chem. Thermodyn. 40, 980–990.

Grenthe, I., Plyasunova, A., 1997. On the use of semiempirical electrolyte theories for the modeling of solution chemical data. Pure Appl. Chem. 69, 951–958.

Guillaumont, R., Fanghänel, T., Fuger, J., Grenthe, I., Neck, V., Palmer, D.A., Rand, M.H., Mompean, F.J., Illemassene, M., Domenech-Orti, C., Ben-Said, K., 2003. Update on the Chemical Thermodynamics of Uranium, Neptunium, Plutonium, Americium and Technetium. Elsevier Science, Amsterdam.

Harvie, C.E., Møller, N., Weare, J.H., 1984. The prediction of mineral solubilities in natural-waters - the Na-K-Mg-Ca-H-Cl-SO4-OH-HCO3-CO3-CO2-H2O system to high ionic strengths at 25° C. Geochim. Cosmochim. Acta 48, 723–751.

Hummel, W., Berner, U., Curti, E., Pearson, F., Thoenen, T., 2002. Nagra/PSI Chemical Thermodynamic Data Base 01/01. Universal Publishers, Parkland, Florida, USA.

Kienzler, B., Metz, V., Brendebach, B., Finck, N., Plaschke, M., Rabung, T., Rothe, J., Schild, D., 2010. Chemical status of U(VI) in cemented waste forms under saline conditions. Radiochim. Acta 98, 675–684.

Loser, R., Lothenbach, B., Leemann, A., Tuchschmid, M., 2010. Chloride resistance of concrete and its binding capacity – Comparison between experimental results and thermodynamic modeling. Cem. Concr. Compos. 32, 34–42.

Lothenbach, B., Winnefeld, F., 2006. Thermodynamic modelling of the hydration of Portland cement. Cem. Concr. Res. 36, 209–226.

Matschei, T., Lothenbach, B., Glasser, F.P., 2007. Thermodynamic properties of Portland cement hydrates in the system CaO-Al_2O_3-SiO_2-$CaSO_4$-$CaCO_3$-H_2O. Cem. Concr. Res. 37, 1379–1410.

Moroni, L.P., Glasser, F.P., 1995. Reactions between cement components and U(VI) oxide. Waste Manage. 15, 243–254.

Neck, V., Altmaier, M., Müller, R., Schlieker, M., Fanghänel, T., 2003. Solubility of U(VI) in NaCl and MgCl2 solutions, 9th International Conference on Chemistry and Migration Behaviour of Actinides and Fission Products in the Geosphere, Migration '03, Gyeongju, Korea.

Pitzer, K.S., 1973. Thermodynamics of electrolytes. I. Theoretical basis and general equations. J. Phys. Chem. 77, 268–277.

Pitzer, K.S., 1991. Activity Coefficients in Electrolyte Solutions, 2. ed. CRC Press Inc., Boca Raton, Florida, USA, pp. 75–153.

Plyasunov, A., Fanghänel, T., Grenthe, I., 1998. Estimation of the Pitzer equation parameters for aqueous complexes. A case study for uranium at 298.15 K and 1 atm. Acta Chemica Scandinavica 52, 250–260.

Pointeau, I., Landesman, C., Giffaut, E., Reiller, P., 2004. Reproducibility of the uptake of U(VI) onto degraded cement pastes and calcium silicate hydrate phases. Radiochim. Acta 92, 645–650.

Reardon, E.J., 1988. Ion interaction parameters for $AlSO_4$ and application to the prediction of metal sulfate solubility in binary salt systems. J. Phys. Chem. 92, 6426–6431.

Reardon, E.J., 1990. An ion interaction-model for the determination of chemical-equilibria in cement water-systems. Cem. Concr. Res. 20, 175–192.

Reardon, E.J., 1992. Problems and approaches to the prediction of the chemical composition in cement/water systems. Waste Manage. 12, 221–239.

Ritherdon, B., Phelps, C., Neff, H., Sowder, A.G., Clark, S.B., 2003. Stability of U(VI) solid phases in the U(VI)-Ca^{2+}-SiO_2-OH system. Radiochim. Acta 91, 93–96.

Robie, R.A., Hemingway, B.S., 1995. Thermodynamic properties of minerals and related substances at 298.15 K and 1 bar (105 Pascals) pressure and at higher temperatures, U.S. Geological Survey Bulletin, p. 461.

Rothe, J., Butorin, S., Dardenne, K., Denecke, M.A., Kienzler, B., Loble, M., Metz, V., Seibert, A., Steppert, M., Vitova, T., Walther, C., Geckeis, H., 2012. The INE-Beamline for actinide science at ANKA. Rev. Sci. Instrum. 83.

Rothe, J., Brendebach, B., Bube, C., Dardenne, K., Denecke, M., Kienzler, B., Metz, V., Prüßmann, T., Rickers-Appel, K., Schild, D., Soballa, E., Vitova, T., 2013. Characterization of U(VI)-phases in corroded cement products by micro(μ)-spectroscopic methods. J. Phys. Conf. Ser. 430, 012114, 012111–012115; <http://dx.doi.org/012110.011088/011742-016596/012430/012111/012114>.

RRUFF, Database of Raman spectroscopy, X-ray diffraction and chemistry of minerals. University of Arizona, Department of Geosciences, <http://rruff.info/> (November 2013).

Stronach, S.A., Glasser, F.P., 1997. Modelling the impact of abundant geochemical components on phase stability and solubility of the CaO-SiO_2-H_2O system at 25° C: Na^+, K^+, SO_4^{2} , Cl- and CO_3^{2} . Adv. Cem. Res. 9, 167–181.

Vejmelka, P., Rudolph, G., Kluger, W., Köster, R., 1990. Die Konditionierung radioaktiver Abfallösungen durch Zementierung. In: Vejmelka, P. (Ed.), KfK 4800. Kernforschungszentrum Karlsruhe, Karlsruhe, p. 80.

Wieland, E., Mace, N., Dähn, R., Kunz, D., Tits, J., 2010. Macro- and micro-scale studies on U(VI) immobilization in hardened cement paste. J. Radioanal. Nucl. Chem. 286, 793–800.

Wolery, T.J., 1992. EQ3/6, A Software Package for Geochemical Modeling of Aqueous Systems, UCRL-MA-110662. University of California, Lawrence Livermore National Laboratory.